



CFD study of a twisted blade H-Darrieus wind turbine

Rajat Gupta, Rituraj Gautam, Siddhartha Sankar Deka

Department of Mechanical Engineering, National Institute of Technology, Silchar, Assam, PIN-788010, India.

Abstract

In this paper, a two-dimensional Computational Fluid Dynamics (CFD) study of the performance of a H-Darrieus turbine with three twisted blade had been carried out. The chord length of each blade is 5cm and the blade height is considered to be same for all the rotors. A two dimensional (2D) model of the turbine was designed in CATIA V5R19 software and a k-epsilon turbulence closure was adopted with the unstructured mesh generated around the rotor modeled in GAMBIT 2.3.16. The inlet velocities and the rotational speeds are taken from the experimental results and the CFD analysis was carried out in CFD Code-FLUENT 6.3.26. From the CFD analysis, power coefficient (C_p) and torque coefficient (C_t) at three different H/D ratios of 1.13, 1.31 and 1.55 respectively were calculated and compared with available experimental results. The computational analysis showed that the highest values of C_p (0.525) and C_t (0.95) were obtained at H/D ratios of 1.31 and 1.13 respectively. The deviation of computational C_p from experimental C_p was within $\pm 3.08\%$ and that of computational C_t from experimental C_t was within $\pm 1.106\%$. A study of the flow behaviour around the rotor was also carried out using the pressure contours and velocity vectors plots. A maximum pressure drop is obtained for H/D ratio of 1.31 and a vortex reattachment near rear blade of rotor with H/D ratio of 1.31 was observed from the pressure contours and velocity vectors plots. The vortex attachment to the blade of the rotor enhances the lift coefficient of the rotor which helps in improving the power coefficient of the rotor. The comparison between the computational results and previous experimental work is pretty encouraging.

Copyright © 2014 International Energy and Environment Foundation - All rights reserved.

Keywords: CFD; H-Darrieus; TSR; Power coefficient; Velocity contour.

1. Introduction

With the exponential rise in use of fossil fuel there has been a rapid depletion of these non-renewable sources of energy. Besides, increasing pollution & global warming have forced environmentalist and energy researchers to vote against these non-renewable sources as the energy source of future. So there began a widespread research in the field of renewable sources of energy which can help in realizing a secure energy future. It is clean in nature and its abundant availability along with the ease with which it can be converted to other forms of energy.

Wind turbines are of two types, Horizontal axis Wind Turbine (HAWT) and Vertical Axis Wind Turbine (VAWT). The original H-Darrieus wind turbine was originally invented and patented by G.J.M Darrieus, a French aeronautical engineer in the year of 1931 [1]. Two types of Darrieus rotors are mainly available, namely troposkien (Egg beater) Darrieus rotor and H-Darrieus rotor. H-Darrieus is a lift type vertical axis wind turbine consisting mainly of two to three airfoil shaped blades which are attached vertically to the central shaft through support arms. It is self-starting and Omni directional.

Due to the progress in computer technology, Computational Fluid Dynamics (CFD) is now able to simulate the fluid flow at moderate costs and time-to solution. The prospect and success of CFD will therefore depend on the accuracy of the approach, in particular the predictive realms of the employed physical models. The interaction of the wind and the blades of the turbine results in the formation of vortices generated both at the upwind and downwind passage near the wind turbine; which is now possible to study very easily due to CFD else complex & time consuming experiments need to be carried out. Though a considerable amount of research had been carried out in the field of design and analysis of VAWT [2-5] but very few literatures can be found in Wind Turbine Community regarding the CFD approaches in H-Darrieus wind turbines. Considerable improvement in the understanding of VAWT can be achieved through the use of Computational Fluid Dynamics and experimental measurements [6].

This paper had attempted to study the numerical aspects of a modified H-Darrieus wind turbine. The present study is confined to incompressible and steady flow around the wind turbine. Pre-processing was carried out in GAMBIT 2.3.16 software for generating the two dimensional mesh. The governing N-S (Navier-Stokes) equations (the continuity equation and the momentum equation) were solved in FLUENT 6.3.26 and for post processing the TECPLOT software was utilized. The results obtained with unstructured mesh were fairly in agreement with the experimental results with minimum difference between the experimental and CFD results. The use of unstructured grids has two major advantages over structured grids in case of modeling the mesh around a VAWT. First, the unstructured mesh allows for fast and efficient grid generation around highly complex geometries like the rotor of the turbine. Second, appropriate unstructured-grid data structures facilitate the insertion and deletion of points and enable the computational mesh to locally adapt to the flow field solution. This means that a very fine grid can be obtained in the immediate vicinity of the rotor which can correctly model the vortices and pressure variation; hence the numerical dissipation can be avoided.

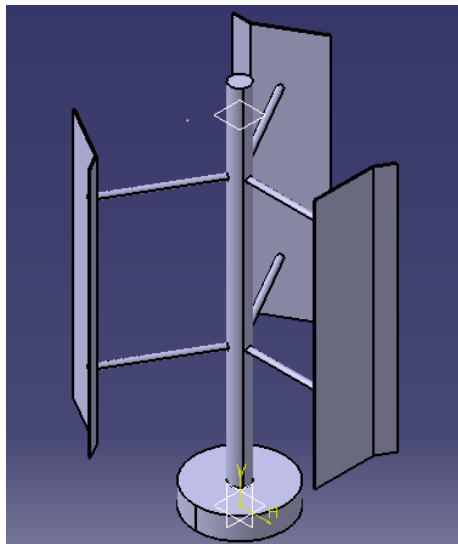
2. Description of the rotor model

The H-Darrieus rotor was 25cm in height and 5cm in chord length. It was twisted with an angle of 30° at the trailing end to make it self-starting from no load condition. Blade thickness was 5 mm. The blades of the rotor were straight length wise and are 120° apart. Three different rotors with different H/D ratios namely 1.13, 1.31 and 1.55 with constant height but with different diameter of the rotor were modeled in CATIA V5R19. The isometric view and top view of a particular rotor model is shown by Figures 1(a) and 1(b) respectively whereas the blade profile of the H-Darrieus rotor is shown by the Figure 1(c). The experimental results were obtained from the experiments conducted by Kakati and Kakati [7] to study the performance of H-Darrieus Wind Turbine rotor in both normal and skewed flow conditions in the wind tunnel present in Mechanical Engineering Department of NIT Silchar. A brief description of the subsonic wind tunnel is provided in the paper [8].

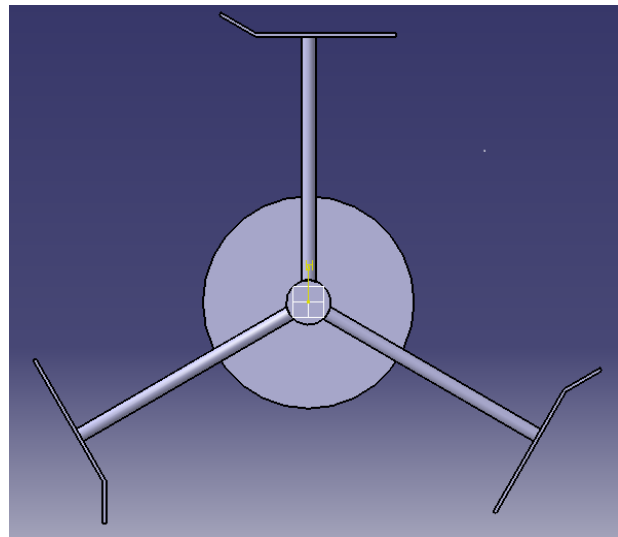
3. Computational methodology

3.1 Computational domain

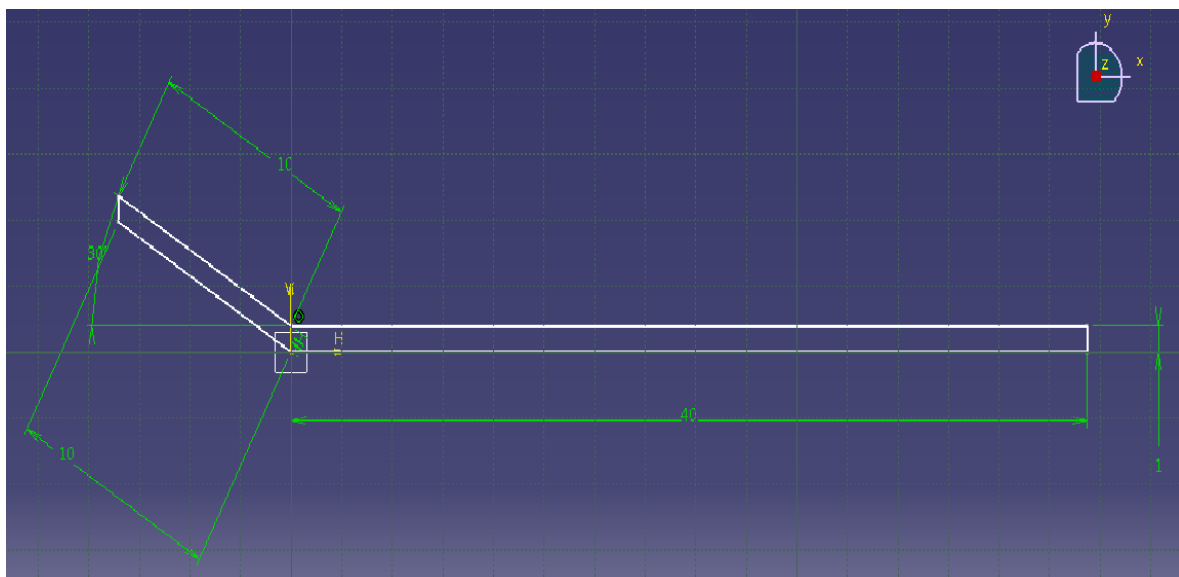
The computational Fluid Dynamics code FLUENT was utilized for solving the N-S equations and GAMBIT was used for generating the two dimensional unstructured mesh. Figure 2 shows the computational domain, which has the three-bladed rotor along with surrounding four edges resembling the test section of the wind tunnel. The unstructured triangular meshing is used for discretizing the computational domain shown in Figure 3. Velocity inlet and outflow conditions were taken on the left and right boundaries respectively. The inlet and outlet BCs were defined considering the wind speed in inlet at on-design value for each rotor to be fixed [9, 10] so that the calculated torque is function of rotational speed only and thereby simplifying the C_p versus λ comparison. The top and bottom boundaries, which signify the sidewalls of the wind tunnel, had symmetry conditions on them. The Symmetry BC is useful because it allows the solver to consider the wall as part of a larger domain, like a 'free shear slip wall', avoiding in this way the wall effects [11]. The blades, shaft and the support arms were set to moving wall conditions. The H-Darrieus wind turbine blades rotate in the same plane as the approaching wind. Moreover, the for an H-Darrieus wind turbine the geometric properties of the blade cross section are usually constant with varying span unlike that of a Darrieus rotor for which the geometric properties vary with the local radius.



(a) An isometric view of the rotor model



(b) A top view of the rotor model



(c) A sketch of the blade profile (all dimensions in mm)

Figure 1. The CAD model of the rotor and the blade profile conceived in CATIA V5R19

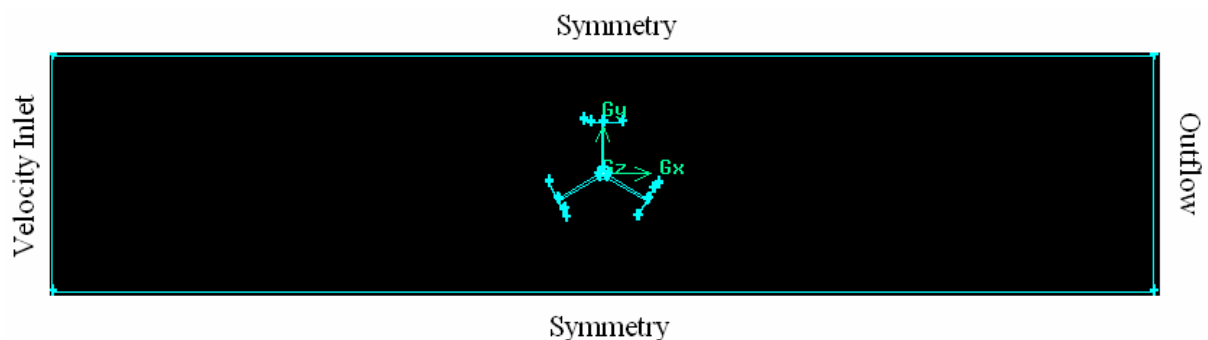


Figure 2. Physical model, boundary conditions and computational domain of the 3-bladed H-Darrieus Rotor for $H/D = 1.13$

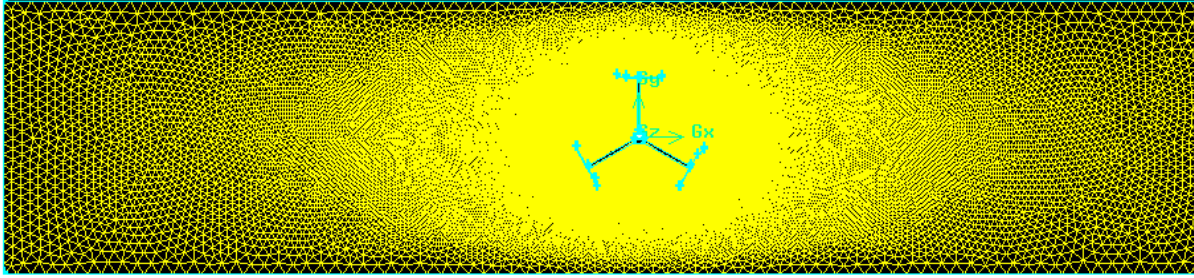


Figure 3. Computational domain after discretization for $H/D = 1.13$

3.2 CFD solver description

The commercial code FLUENT 6.3.26 was used for performing the CFD analysis for Reynolds number of the order 3×10^5 . A steady state segregated solver with absolute velocity and implicit formulation and Green Gauss cell-based gradient option was considered. The FLUENT default segregated solver helps in solving the governing integral equations for continuity and momentum sequentially. For the 2D, steady and incompressible flow the continuity equation is:

$$\frac{\partial U}{\partial X} + \frac{\partial V}{\partial Y} = 0 \quad (1)$$

Momentum equation for viscous flow in X direction:

$$U \frac{\partial U}{\partial X} + V \frac{\partial U}{\partial Y} = -\frac{1}{\rho} \frac{\partial P}{\partial X} + \frac{\partial}{\partial Y} \left[(\nu + \nu_t) \frac{\partial U}{\partial Y} \right] \quad (2)$$

In the above equation $\frac{\partial U}{\partial X}$, $\frac{\partial V}{\partial X}$ indicates velocity gradient along x and y direction respectively whereas

$\frac{\partial P}{\partial X}$ indicates rate of pressure variation along x direction and ν , ν_t represents the dynamic viscosity. As the governing equations are non-linear, several iterations must be performed before a converging solution is obtained. A flow chart (Figure 4) is illustrated how the iterations are carried out. The fluid properties are updated initially based on initialized solution.

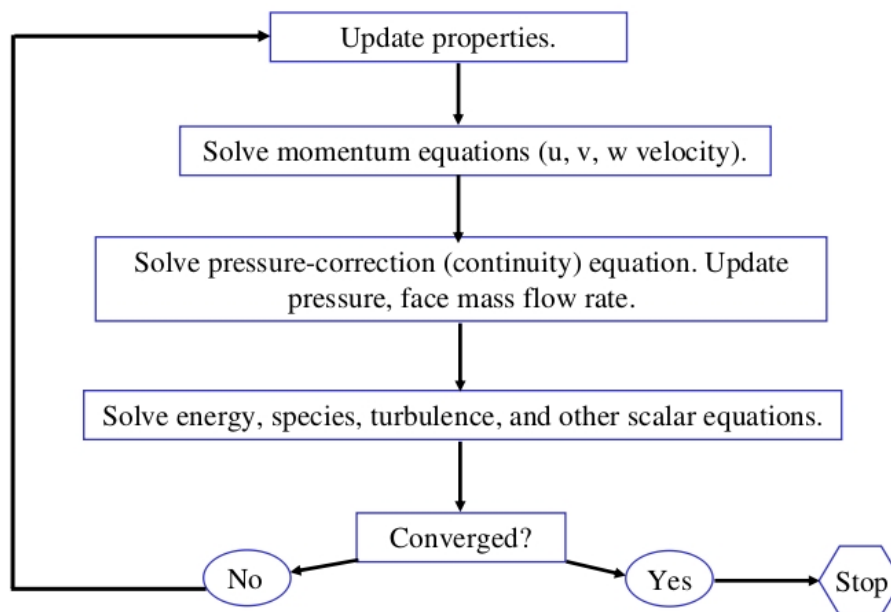


Figure 4. Overview of the segregated solution method

A second order upwind discretization scheme was adopted for momentum discretization and SIMPLE (Semi-Implicit Method for Pressure Linked Equations) algorithm was used for pressure velocity coupling of the flow. When the second order upwind discretization is used the quantities at the cell faces are computed using a multidimensional reconstruction approach as proposed by Barth and Jespersen [12]. The SIMPLE algorithm [13] converts the continuity equation into a discrete Poisson equation for pressure. The differential equations are linearized and solved implicitly in sequence: starting with pressure equation (predictor stage), followed by momentum equations and the pressure correction equation (corrector stage). The equation of the scalars (turbulent quantities) is solved after updating of both pressure and velocity components. The iterations were done to achieve a converged solution. Implicit formulation is used for linearizing the non-linear governing equations to produce a system of equations for the dependent variables for every computational cell. In the segregated method each governing equation is linearized implicitly with respect to that equation's dependent variable. This will result in a system of linear equations with one equation for each cell in the domain. A Gauss-Siedel linear equation solver is used in colligation with an Algebraic Multigrid method to solve the resultant systems of equations for the dependent variable in each cell. Gradients are needed for computing secondary diffusive terms, velocity derivatives as well as for constructing values of all scalar variables at the cell faces. Green- Gauss Cell based had been considered for computing the gradients. The turbulence in the flow was modeled using a standard k- ϵ viscous model with standard wall functions was chosen. The standard wall functions give reasonably accurate predictions for the majority of high-Reynolds-number, wall-bounded flow & is also accurate for far field flows. The standard wall functions are based on the proposal by Launder and Spalding [14]. The two equation k- ϵ turbulence model is the simplest one and is widely used to solve the two separate transport equations to allow the turbulent kinetic energy and its dissipation rate to be independently determined. The model is reasonably accurate and computationally less expensive. The governing equations were integrated over each control volume to construct discretized algebraic equations for dependent variables. The transport equations for k and ϵ in the standard k- ϵ model [11] are as given below:

Turbulent kinetic energy (k) equation:

$$\frac{\partial}{\partial t}(\rho k) + \frac{\partial}{\partial x_i}(\rho k u_i) = \frac{\partial}{\partial x_j} \left[\left(\mu + \frac{\mu_t}{\sigma_k} \right) \frac{\partial k}{\partial x_j} \right] + P_k - \rho \epsilon - Y_M \quad (3)$$

For dissipation (ϵ):

$$\frac{\partial}{\partial t}(\rho \epsilon) + \frac{\partial}{\partial x_i}(\rho \epsilon u_i) = \frac{\partial}{\partial x_j} \left[\left(\mu + \frac{\mu_t}{\sigma_\epsilon} \right) \frac{\partial \epsilon}{\partial x_j} \right] + C_{1\epsilon} \frac{\epsilon}{k} (P_k) - C_{2\epsilon} \frac{\rho \epsilon^2}{k} \quad (4)$$

Model constants:

$$C_{1\epsilon} = 1.44, C_{2\epsilon} = 1.92, C_\mu = 0.09, \sigma_k = 1.0, \sigma_\epsilon = 1.3$$

Modeling turbulent viscosity:

$$\mu_t = \rho C_\mu \frac{k^2}{\epsilon} \quad (5)$$

Production of k due to mean velocity gradients:

$$P_k = -\rho \bar{u}_i' \bar{u}_j' \frac{\partial u_j}{\partial x_i} \quad (6)$$

In these equations, P_k represents generation of turbulent kinetic energy due to mean velocity gradients, the turbulent Prandtl Numbers σ_k and σ_ϵ is for k and ϵ respectively. All the variables including turbulent kinetic energy k , its dissipation rate ϵ were shared by each fraction of fluid volume.

The philosophy behind adopting RANS (k - ϵ model) is that in it the Navier-Stokes equations are decomposed into time-averaged and fluctuating components. This yields a turbulence simplification that reduces computational demands from the LES/DES, and still achieves acceptable accuracy for complex flow. The details of the solution strategy adopted is provided in Appendix.

3.3 Grid independence test

The correctness of the computational results depends upon the resolution of the grid. However very fine resolution of the mesh results in increased computational cost leading to higher time consumption and money. It can be seen that with gradually refining of the mesh (or improved grid density) the variation in the results obtained computationally is very less after a while it becomes nil. At this point a limit of the refinement of the mesh is reached and further refinement would not have any effect in the results. In the analysis C_d had been chosen as the parameter to obtain the Grid Independence Limit. Grid refinement is carried out until a steady value of C_d is obtained. From the grid independence test it can be clearly seen that the value of C_d is constant beyond 68369 nodes (Figure 5). So the mesh with 121657 nodes & skewness less than 0.5 is being considered for the final simulation.

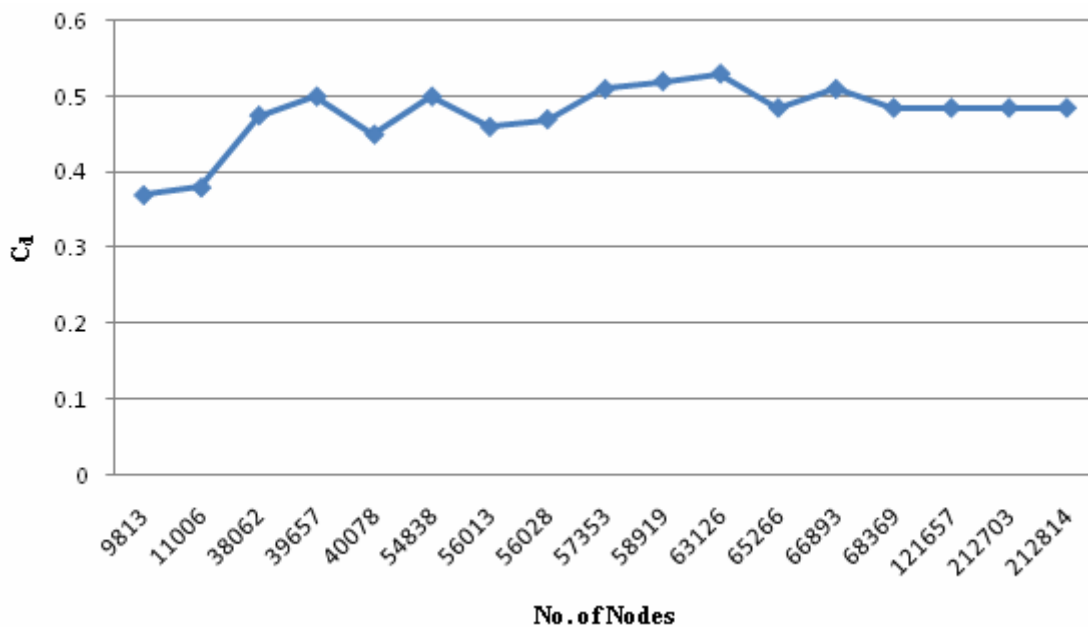


Figure 5. Grid independence test carried out for the 3-bladed H-Darrieus rotor

4. Analysis of results

The experimental and computational C_p and C_t with respect to tip speed ratio and the percentage deviations of the computational results from the experimental results for various H/D ratios are calculated as below [15].

$$C_t = \frac{T}{\frac{1}{4} \rho A V_{free}^2 D} \tag{7}$$

$$C_p = \frac{T \omega}{\frac{1}{2} \rho A V_{free}^3} \tag{8}$$

Now putting the value of torque from equation (7) in (8)

$$C_p = \frac{1}{2} C_t \frac{D\omega}{V_{free}} \quad (9)$$

Tip Speed Ratio (TSR) is given by

$$\lambda = \frac{\text{Tip Speed of Blade}}{\text{Wind Speed}} = \frac{C_p}{C_t} = \frac{\pi DN}{60V_{free}} \quad (10)$$

In the above equations, the values of C_t (torque coefficient) and C_p (power coefficient) are known after FLUENT analysis. The difference of the experimental and computational results had been calculated in the form of standard deviation from the data set for each set of H/D ratios. The standard deviation formula used for power coefficient is

$$\sigma^2 = \frac{1}{n-1} \left[\sum_{i=1}^n (C_{p_i} - \overline{C_p})^2 \right] \quad (11)$$

where,

$$\overline{C_p} = \frac{1}{n} \sum_{i=1}^n C_{p_i} \quad (12)$$

Here σ is the standard deviation and n is the number of data taken.

A comparison of the experimental and computational values of C_p and C_t for different values of H/D ratios is shown by Figures (6, 8, 10, 12, 14 and 16). The standard deviation of the computational C_p and C_t values from the experimental ones is shown by Figures (7, 9, 11, 13, 15 and 17). Finally Figures 18, 19 show the maximum values of C_p and C_t , both computational and experimental for the three different H/D ratios.

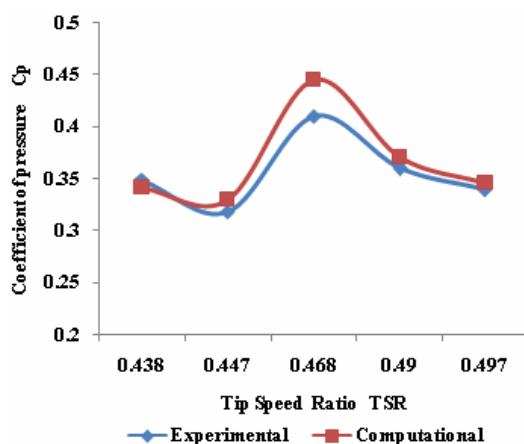


Figure 6. Variation of C_p with TSR for H/D=1.13

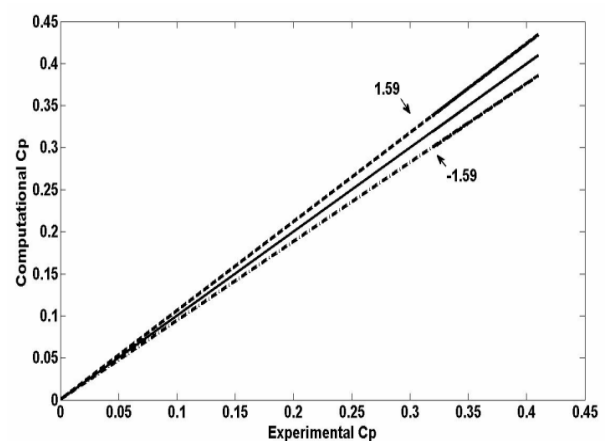


Figure 7. Deviation of computational C_p from experimental C_p for H/D=1.13

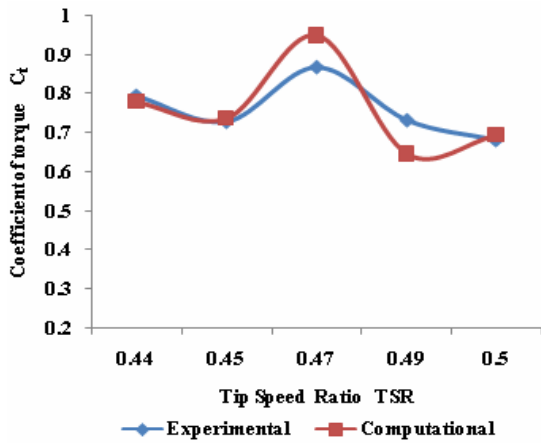


Figure 8. Variation of C_t with TSR for $H/D=1.13$

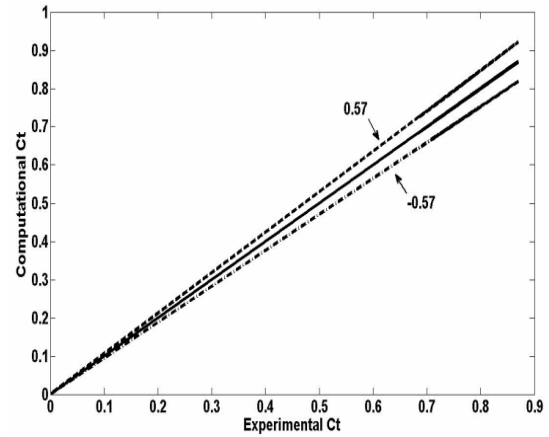


Figure 9. Deviation of computational C_t from experimental C_t for $H/D=1.13$

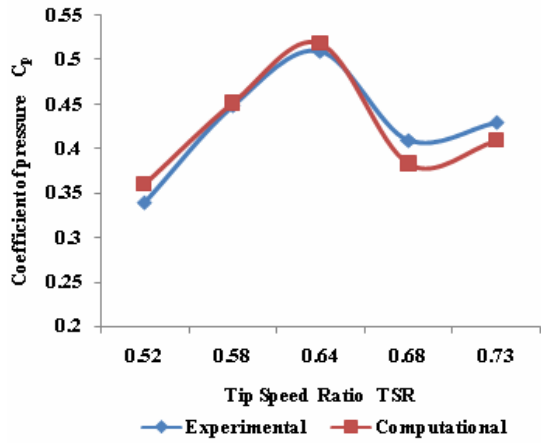


Figure 10. Variation of C_p with TSR for $H/D=1.31$

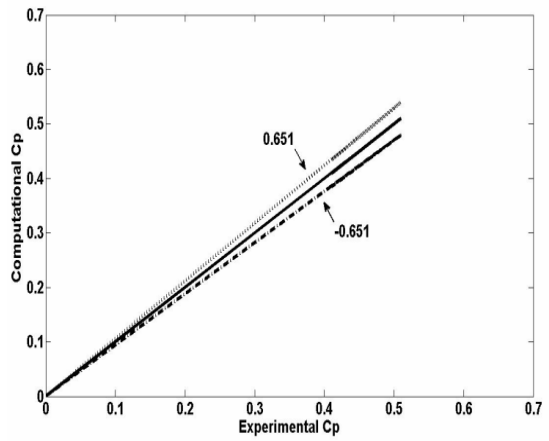


Figure 11. Deviation of computational C_p from experimental C_p for $H/D=1.31$

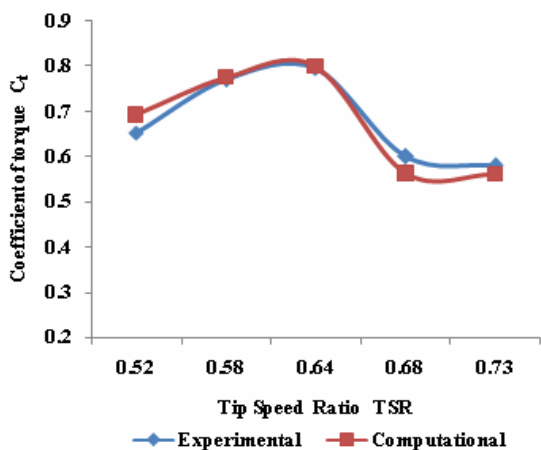


Figure 12. Variation of C_t with TSR for $H/D=1.31$

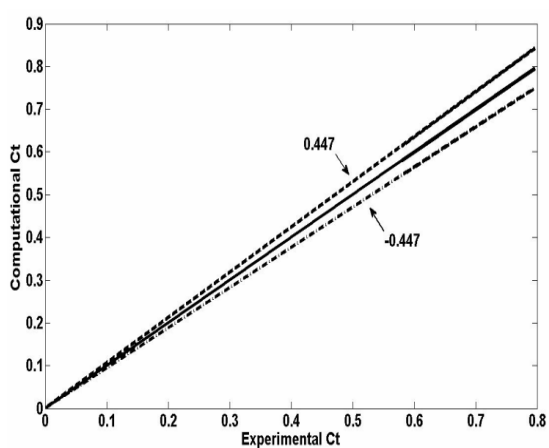


Figure 13. Deviation of computational C_t from experimental C_t for $H/D=1.31$

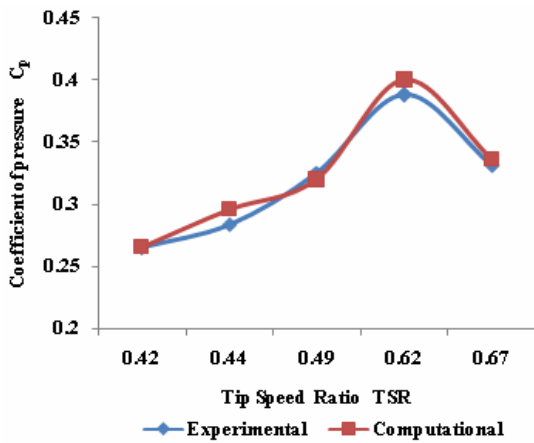


Figure 14. Variation of C_p with TSR for $H/D=1.55$

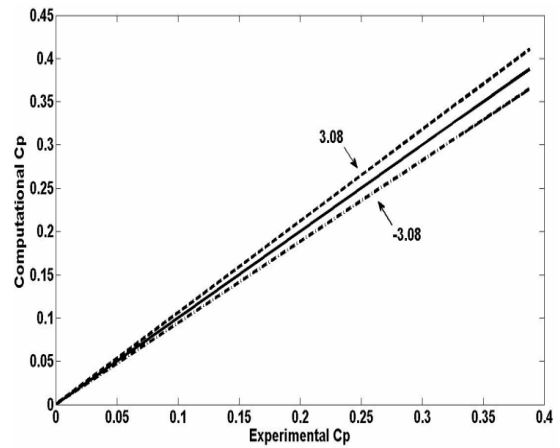


Figure 15. Deviation of computational C_p and experimental C_p for $H/D=1.55$

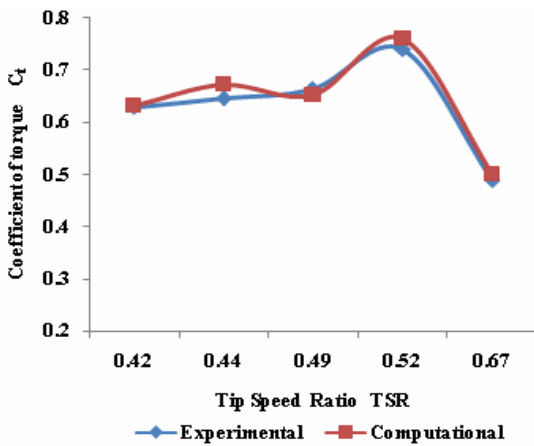


Figure 16. Variation of C_t with TSR for $H/D=1.55$

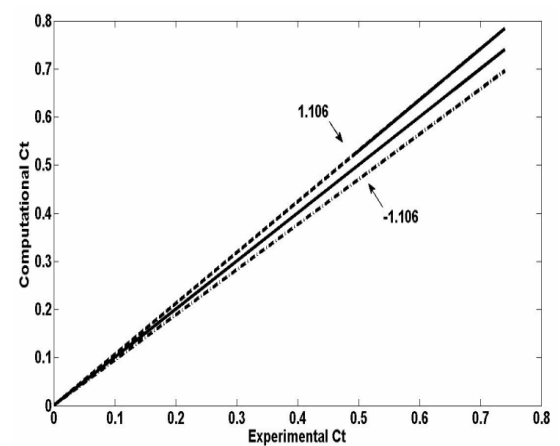


Figure 17. Deviation of computational C_t and experimental C_t for $H/D=1.55$

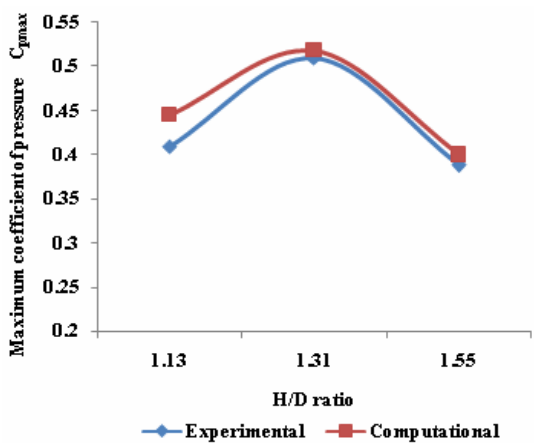


Figure 18. Comparison between experimental and computational C_p for different H/D ratios

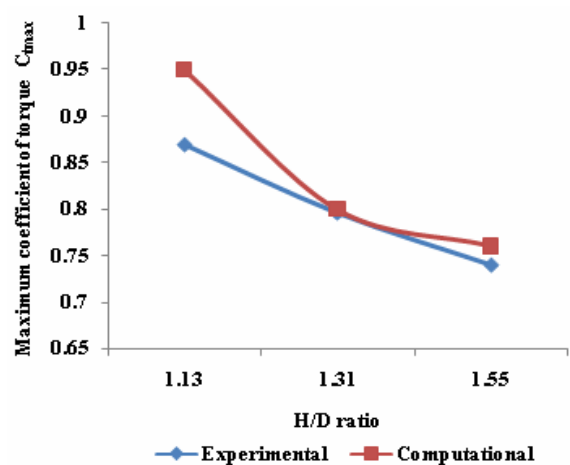


Figure 19. Comparison between experimental and computational C_t for different H/D ratios

4.1 Comparison of experimental and computational results

From Figures 6 and 8, it is found that, for H/D ratio 1.13, the maximum C_p obtained is 0.445 at a TSR of 0.477, and the maximum C_t obtained is 0.95 at a TSR of 0.471. And for this H/D ratio, the standard deviation (Figures 7 and 9) of computational C_p from experimental C_p is 1.59% and that of computational C_t from experimental C_t is 0.57%. From Figures 10 and 12, it is found that, for H/D ratio 1.31, the maximum C_p obtained is 0.518 at a TSR of 0.643, and the maximum C_t obtained is 0.80 at a TSR of 0.652. And the standard deviation (Figures 11 and 13) of computational C_p from experimental C_p is 0.651% and that of computational C_t from experimental C_t is 0.447%. From Figures 14 and 16, it is found that, for H/D ratio 1.55, the maximum C_p obtained is 0.40 at a TSR of 0.526, and maximum C_t obtained is 0.76 at a TSR of 0.533; the standard deviations (Figures 15 and 17) of C_p and C_t are 3.08% and 1.106% respectively. From Figure 18, it can be found that the maximum computational C_p of 0.518 and maximum experimental C_p of 0.51 occur for H/D ratio of 1.31. Also from Figure 19, the maximum computational and experimental C_t comes out to be 0.95 and 0.87 respectively for H/D ratio corresponding to 1.13. From Figures 6-19 it can be clearly be interpreted that there is a close concurrence of the computational and experimental results.

4.2 Pressure contours and velocity vectors analysis for different H/D ratios

Post processing of the results after solving the governing equations is obtained in Tecplot 360. From the Figures 21, 23 and 25 it can be observed the velocity magnitude vectors and Figures 20, 22 and 24 represents the pressure contours of the three bladed H-Darrieus rotor for three different H/D ratios, namely 1.13, 1.31 and 1.55. The flow is mainly affected downstream of the rotor, while the flow upstream of the rotor almost remains unaffected except for the regions very near to the rotor. The velocity vectors show that the flow is accelerated while passing over the rotor blades. The velocity at the blade tips is almost 1.8 times higher compared to the input velocity on the extreme left of the computational domain. This velocity gradient generates the power stroke of the blades during its clockwise rotation. In case of wind turbines the highest aerodynamic torque at is developed at the blade tips and the high velocity magnitude at the blade tips ensures augmentation in aerodynamic torque production. Further, the velocity vectors show that, with the increase of H/D ratio, the velocity magnitude difference from inlet up to the rotor increases up to a certain H/D ratio and then decreases meaning loss of performance for the turbine with increase of H/D ratio. As is evident from Figure 18 it can be seen that the C_p value increases initially with increase of H/D ratio from 1.13 to 1.31 and then decreases with further increase of H/D ratio from 1.31 to 1.55. For example at H/D ratio of 1.13, there is a velocity drop of 16.71m/s which increases to 25.67 m/s for H/D ratio of 1.31 but when the H/D ratio of 1.55 is considered the velocity drop decreases to 11.9 m/s. This fact is further supplemented with the observation that maximum static pressure drop of 1990 Pa is observed for H/D ratio of 1.31 as shown in Figure 22 and minimum static pressure drop for H/D ratio of 1.55 around 1395Pa as shown in Figure 24. This occurrence enhances the aerodynamic torque of the rotor and improves the power extraction of the rotor of H/D ratio 1.31 to maximum. This is in agreement with the work done on two bladed H-Darrieus rotor by Gupta et al. [16] where it was shown that the power extraction of the two bladed H-Darrieus rotor increases with increasing H/D ratio to 1.0 and beyond that there is a fall in power coefficient. From the velocity vectors plot it is pretty evident that vortices are formed close to the rotor. These clockwise rotating vortices formed on the rear side of the rotor gradually grows in size for increasing H/D ratio up to 1.31 but it becomes smaller on approaching H/D ratio of 1.55. Another interesting observation is that for the blade downstream of the flow the vortices are separated for H/D ratios of 1.13 and 1.55 but are attached to the blade in case H/D ratio of 1.31. Also not much variation in velocity can be found in the vortex region between the approaching blades in case of H/D ratio of 1.31. However a variation in velocity is observed for H/D ratio of 1.13 and 1.55.

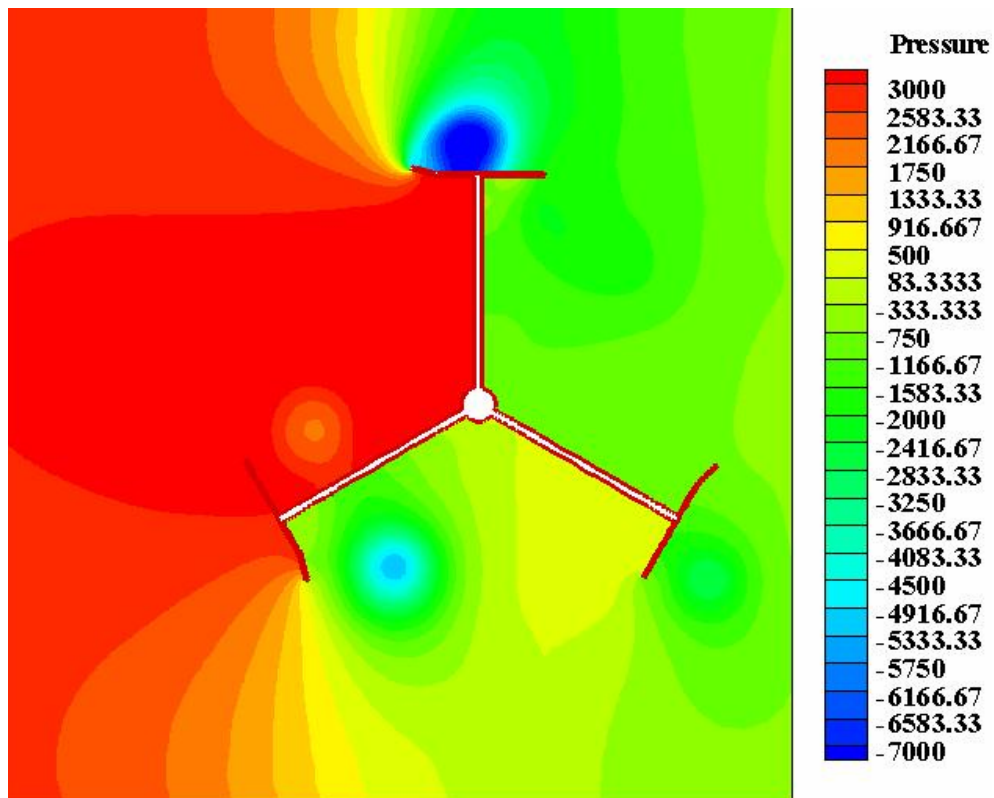


Figure 20. Pressure (Pa) contours for $H/D=1.13$

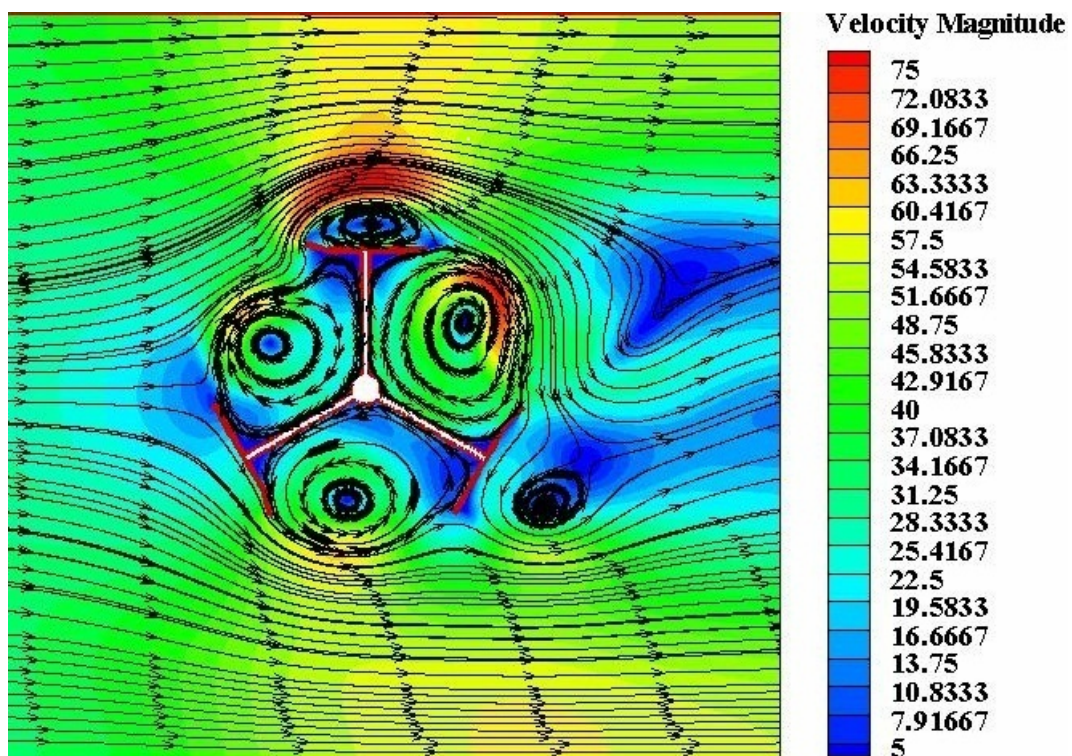


Figure 21. Contours of velocity magnitude (m/s) along with streamlines for $H/D=1.13$

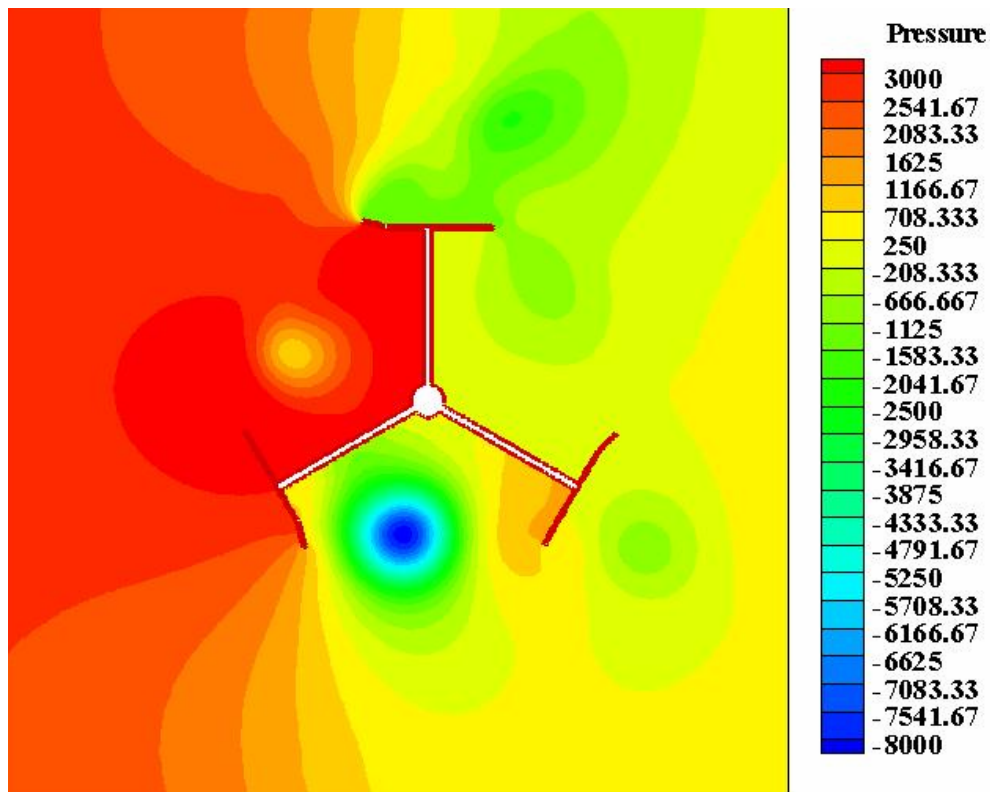


Figure 22. Pressure (Pa) contours for $H/D=1.31$

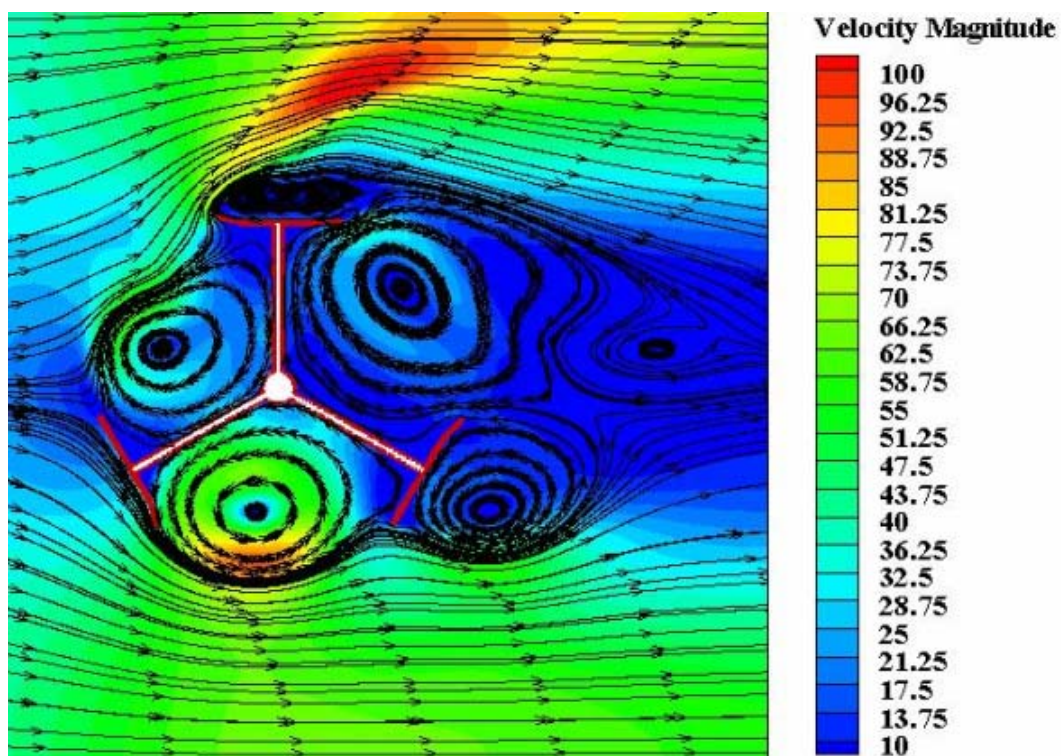


Figure 23. Contours of velocity magnitude (m/s) along with streamlines for $H/D=1.31$

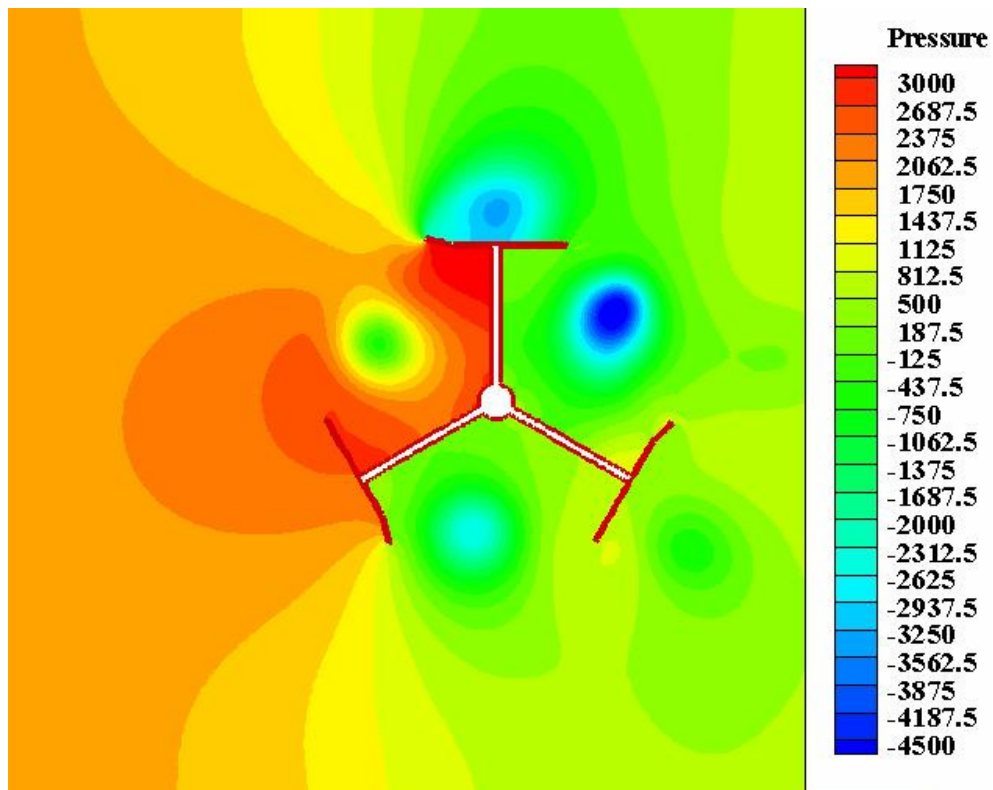


Figure 24. Pressure (Pa) contours for $H/D=1.55$

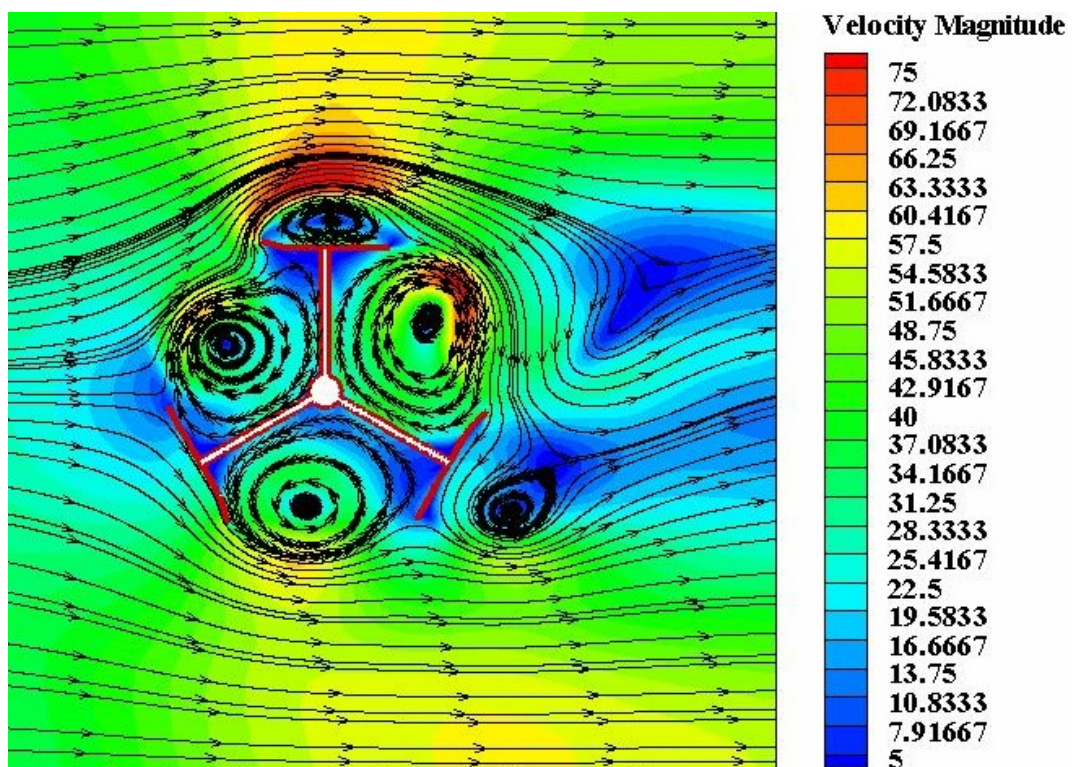


Figure 25. Contours of velocity magnitude (m/s) along with streamlines for $H/D=1.55$

5. Conclusion

The power coefficients and torque coefficients of the H-Darrieus rotor were evaluated numerically using CFD for three different H/D ratios. A comparative study was followed between the experimental and computational results. It was found that there was a close conformity between the computational and experimental results. The deviation of computational C_p from experimental C_p was within $\pm 3.08\%$, whereas the deviation of computational C_t from experimental C_t was within $\pm 1.106\%$. These findings highlight the potential of CFD as a tool for the performance measurement of vertical axis wind rotor and go a step forward in establishing the fact that the standard k- ϵ turbulence model can predict the flow behaviour in steady state analysis of VAWTs with a 2D rotor model (for a $Re\ 3 \times 10^5$ of the flow) within $\pm 3.08\%$. From the contour plot analysis, it is observed that velocity at the blade tips is quite high compared to the input velocity. With increase in H/D ratio from 1.13 to 1.31 the velocity drop across the rotor increases and becomes the maximum at H/D of 1.31 thereby suggesting maximum performance at this H/D ratio. But beyond H/D ratio of 1.31 the velocity drop and hence the power extraction decreases as being clearly evident from the rotor with H/D ratio of 1.55. The k epsilon model had also been able to closely predict the formation of the vortices near the blade. In case of the rotor with H/D ratio of 1.31, an attachment of the vortices is seen near the rear blade on the downstream side of the rotor. These are very strong vortices and an extremely low pressure region is formed in the centre of the vortices. The generation of the vortices improves in the lift coefficient of the rotor. Due to the increased lift coefficient an increment in the power coefficient of the rotor with ratio of H/D ratio is seen.

Appendix:

Solution specifications

Solver:

- Solver: Pressure Based
- Time: Steady
- Space: 2D
- Formulation: Implicit

Viscous Model:

- Model: Standard k-epsilon (k- ϵ)
- Near-Wall Treatment: Standard Wall Functions
-   Material: Air ($\mu = 1.7894 \times 10^{-5}$ kg/m-s, $\rho = 1.225$ kg/m³)

Operating conditions: Atmospheric Pressure (1.0132 bar)

Boundary Conditions:

- Inlet: Velocity Inlet
- Sides: Symmetry
- Rotor Blades: Moving Wall
- Outlet: Outflow

Solution controls:

- Pressure Velocity Coupling: SIMPLE
- Under Relaxation Factor: 0.7 (Momentum)
- Discretization: Momentum (Second Order Upwind) for pressure velocity coupling, Pressure (Standard)

Solution Initialization: Inlet condition

Residual Monitors: 0.001 (continuity, x-velocity, y-velocity, k, ϵ)

Force Monitors: Drag Coefficient

Inlet Velocity: 31.3 m/s

References

- [1] G.J.M Darrieus, Turbine having its rotating shaft transverse to the flow of the current, US Patent no. 1.835.018, 1931.
- [2] S. Mertens and E. de Vries, "Small Wind Turbines: Driving Performance", Renewable Energy World, 11: Issue 3, 2008.
- [3] A. Iida, K. Kato, A. Mizuno, in Numerical Simulation of Unsteady Flow and Aerodynamic Performance of Vertical Axis Wind Turbines with LES: Proceedings of the 16th Australian Fluid Mechanics Conference, Crown Plaza, Gold Coast, Australia, 2-7 December 2007.
- [4] D.P. Coiro and C. de Nicola, in Prediction of Aerodynamic Performance of Airfoils in Low Reynolds Number Flows: Proceedings of the Low Reynolds Number Aerodynamics Conference, Notre Dame, Indiana, USA, 5-7 June, 1989.
- [5] L. P. Fernando, M. J. Pablo, A vortex model for Darrieus turbine using finite element techniques, Journal of Renewable Energy, pp 1–18, vol.24, 2001.
- [6] R. Howell, N. Qin, J. Edwards, N. Durrani, Wind tunnel and numerical study of a small vertical axis wind turbine, Renewable Energy Journal, 35, 412-422 (2010).
- [7] J.Kakati and H.Kakati, Study of the performance of H-Darrieus Wind turbine in both normal and skewed flow conditions, B.Tech Thesis, NIT Silchar, India, 2007.
- [8] R. Gupta, R. Das, K. K. Sharma, Experimental study of a Savonius-Darrieus wind machine: Proceedings, International Conference on Renewable Energy for Developing Countries, Washington DC, USA, 2006.
- [9] Bravo R., Tullis S., Ziada S. Performance Testing of a Small Vertical-Axis Wind Turbine. Mechanical Engineering Department, McMaster University
- [10] Takao M., Kuma H., Maeda T., Kamada Y., Oki M., Minoda A. A Straight-bladed Vertical Axis Wind Turbine with a Directed Guide Vane Row - Effect of Guide Vane Geometry on the Performance - Journal of Thermal Science Vol.18, No.1 (2009) 54–57
- [11] Ferziger J.H., Peric M. Computational methods for fluid dynamics. Springer.
- [12] T. J. Barth and D. Jespersen, The design and application of upwind schemes on unstructured meshes, Technical Report AIAA-89-0366, AIAA 27th Aerospace Sciences Meeting, Reno, Nevada, 1989.
- [13] S.V. Patankar, Numerical Heat Transfer and Fluid Flow. Hemisphere, Washington, D.C, 1980. ISBN 0-89116-522-3.
- [14] B. E. Launder and D. B. Spalding, The Numerical Computation of Turbulent Flows, Computer Methods in Applied Mechanics and Engineering, 3pp. 269-289, 1974.
- [15] R.Gupta, A.Biswas, K.K.Sharma, Comparative study of a three-bucket Savonius rotor with a combined three-bucket Savonius–three-bladed Darrieus rotor, Journal of Renewable Energy, (2008).
- [16] R. Gupta, S. Roy, A. Biswas, Computational fluid dynamics analysis of a twisted airfoil shaped two-bladed H-Darrieus rotor made from fibreglass reinforced plastic (FRP), International Journal of Energy and Environment, ISSN 2076-2909 (Online) Volume 1, pp.953-968 (Issue 6, 2010).



Rajat Gupta, a PhD from Indian Institute of Technology Delhi, has been a Professor in Mechanical Engineering Department at NIT Silchar since 1996. About 114 papers of his have been published in various national/international journals/conferences. His research interests include wind turbines, CFD, material science, productivity studies of mechanical systems, entrepreneurship development etc. He guided quite a number of M.Tech students and also guided three PhD scholars in his research field. Presently he is guiding two PhD students. His teaching interests include fluid mechanics, hydraulic machines, CFD, entrepreneurship development, material science etc. Professor Gupta worked in many important administrative posts in NIT Silchar, like Director (In-charge), Dean (Research & Consultancy), Dean (Students Welfare), Chief Wardens and many more. He is currently holding the post of Director of NIT Srinagar, Hazratbal, Srinagar (J & K).
E-mail address: rguptanitsri@gmail.com



Rituraj Gautam did his B.Tech in Mechanical Engineering from National Institute of Technology, Silchar. Currently he is working in Vehicle NVH group in Maruti Suzuki India Ltd. His research interest primarily lies in the field of CFD, VAWTs & automotive NVH.
E-mail address: riturajgautam030@gmail.com



Siddhartha Sankar Deka Dekadid did his B.Tech in Mechanical Engineering from National Institute of Technology, Silchar. Currently he is working as an Automotive Transmission Design Engineer at Mahindra & Mahindra Ltd. His Research interests lie primarily in the field of Numerical Methods, CFD, Wind Turbines, Automotive Transmission Design.
E-mail address: ssdeka.nits@gmail.com